Alma Mater Studiorum · Università di Bologna

SCHOOL OF SCIENCE
Telecommunication Engineering

NUMERICAL ANALYSIS ON THE EFFECT OF FOCUSING METASURFACES IN ENERGY HARVESTING APPLICATIONS

Supervisor:
Prof. Diego Masotti

Co-supervisor:
Dr. Enrico Fazzini
Prof. Lina Mroueh

Presented by:
Federico Ricci Lucchi

Session
2022-23

Contents

1 Introduction

1.1 Introduction to Wireless Energy Harvesting

In the reality of wireless power transmission there are multiple methods to transmit power wirelessly. They differ themselves based on the nature of their application, and can be divided into 2 categories: Wireless Power Transfer and Wireless Energy Harvesting. "Wireless Power Transfer", also known as WPT, it's the technique that actively exchange power between receiver and transmitter. Based on the distance, and therefore the working region, of the two antennas, different techniques are utilized. In case of Near-Field Wireless Power Transfer (NF-WPT) the strong coupling between coils is exploited to transfer high amounts of energy over the link. Instead, in the case of Far-Field Wireless Power Transfer (FF-WPT) the energy is transferred thanks to the electromagnetic propagation of the radio-frequency signal that is then rectified in DC power at the receiver side. The system that includes the combination of receiver antenna and rectifier takes the name of "rectenna". "Wireless Energy Harvesting", more commonly referred as WEH, allows to indirectly exchange power between a transmitter and a receiver antenna. Differently from WPT, WEH "harvests", therefore captures, the energy already present in the environment generated by various sources, while in WPT there's a direct transmission of power between the 2 sides.

It's important to note that having different kind of signals causes a variation on the actual captured energy, because the interaction between the signal and the receiver antenna which are not correctly matched will result into a substantial energy loss. Some of the most relevant properties that might influence the harvesting efficiency of the system are: frequency, polarization and direction. Creating a system with the ability of capturing as many different signals as possible represents priority in the design of WEH systems. An example of WEH system is shown in Fig.1.

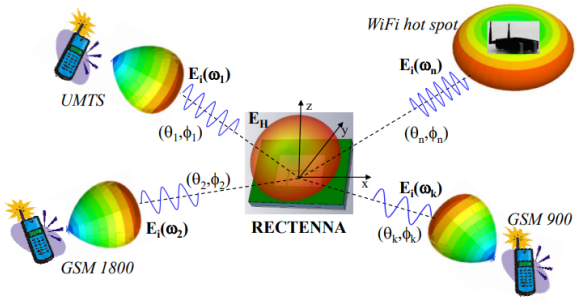

Figure 1: Example of WEH application [1]

Wireless Energy Harvesting compared to Wireless Power Transfer (WPT) technique is different in many ways. In foremost, in WPT systems both transmitter and receiver antennas are designed by the user, while in WEH only the receiving end is under control, that implies that in WPT applications frequency, source direction and polarization are known allowing to transmit much more power over the wireless link, in principle. Matching a wireless link for a wireless energy harvesting applications, instead, results more challenging because there are many variables that cannot be controlled during the design phase, resulting into a lower transferred energy.

The lower harvested energy makes WEH systems suitable for low power consumption wearable devices and sensors. This would allow to remove any backup batteries to make these devices truly independent from any energy storage solution. In recent years, in order to improve the performance in terms of received power for WEH link, the scientific community is investigating and exploiting interest solutions. The most promising one is represented by the metasurfaces. Object of this thesis work is to present a novel metasurface for WEH applications able to profitable exploit the ranging capability, i.e. the possibility of focusing the EM radiation in a confined region of space. The work is organized in the following order:

1. introduction to metasurface technology and its application
2. example of metasurface for absorption application
3. example of metasurface for focusing application
4. introduction and analysis of a new metasurface model for focusing
5. set up of a WEH system to analyze the performance boost given by the metasurface

1.2 What's a Metasurface?

Metamaterial and Metasurfaces (MS) are new and incoming materials that derive their physical properties from their unique geometric organization instead of intrinsic chemical properties. They are mainly used for Wireless Energy Harvesting (WEH) and Wireless Power Transfer (WPT) application with the objective to enhance the total efficiency of the system and can be installed as radomes for antennas. Before giving the Metamaterial's definition, the material's composition must be analyzed. From this analysis, any kind of material falls under one of 4 different categories, based on the values of the constants ε (electric permittivity) and μ (magnetic permeability), as shown in Fig.2.

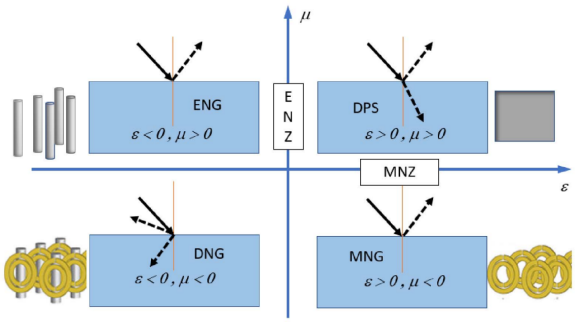

Figure 2: Materials classification [2]

1. Both ε and μ are positive, it is referred as *Conventional double-positive* (DPS) material easily found in nature. The Snell's law, therefore, is respected.
2. ε negative but μ positive, it's a *Epsilon-negative* (ENG) material. Here there's no wave propagation inside the material and most of the energy carried by the wave is reflected. The materials who have this property are usually composed by thin wires.

3. μ negative but ε positive, corresponds to a *Mu-negative* (MNG) material. Here an analog phenomena happens as in the ENG materials where there's no transmitted wave propagating inside the material and all the incident waves are reflected. To build such materials a structure called Split-Ring Resonators (SRRs) is needed.

4. Finally, both ε and μ are negative, most commonly referred as Left-Hand-Materials (LHMs), are *Double-negative* (DNG) material. To replicate such characteristics there's the need of both thin wires and SRRs. Its peculiarity compared to DPS materials it's that the reflected signal is partially reflected into the medium where the signal travels backwards compared to what happens in nature. Such phenomena it's caused by the refractive index (n) being negative in DNG materials, while in ENG and MNG it's purely complex, therefore the signal cannot propagate inside it as it is completely dissipated.

   Being n purely negative implies that the Snell's law it's not valid anymore generating this unusual phenomena where 2 different waves propagates in the opposite direction. Such materials are non-existent in nature but they can be artificially obtained.

Strictly speaking, a material with an effective relative permittivity positive but less than 1 and/or an effective relative permeability positive but less than 1 can also be called a metamaterial. Thus, another property that cannot normally be found in nature but can be achieved with metamaterials is the one with a near-zero refractive index. This could be Epsilon near-zero (ENZ) or Mu near-zero (MNZ) materials. Occasionally, a material with a positive, but extremely high permittivity or permeability is also called a metamaterial [2].
The metamaterial's design start with the building of an unitary element then replicated for obtaining a periodic pattern. The main element, more commonly referred as *unit cell* of the metamaterial, is designed to enhance the interaction between atoms that allows to control its electromagnetic properties: the bigger the periodic structure the stronger the control on the final result.
Metamaterials are usually arranged into a 2-D pattern, often composed of multiple metallic layer, and therefore they are usually referred as Metasurface (MS).

1.3 Metasurfaces applications

The role of metamaterials and metasurfaces is to reduce the shortcomings of WEH and WPT systems, representing a feature to increase the overall link efficiency. With this objective new concepts have been proposed to improve the quality of the received signals.

Many of the solutions that have been proposed consist in using metasurfaces as lens or reflective surfaces able to beamform and range in space the incident wave into a well-defined and consistent point and direction. On the other hand, mainly used for WEH applications, there are structures called *Metasurface absorber* whose main goal it's to optimize the system efficiency by increasing the harvested energy through the interaction between many cells. As shown respectively in Fig.3 and Fig.4 an example of both a focusing and absorber structure is presented. "Metasurface Absorber", also called rectifying metasur-

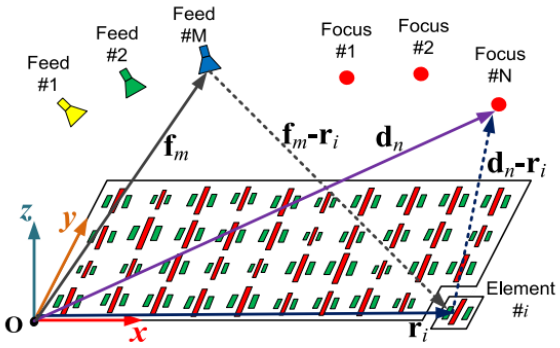

Figure 3: Example of focusing metasurface [2]

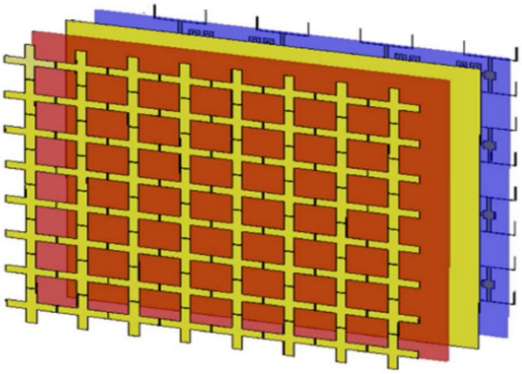

Figure 4: Example of metasurface absorber [2]

faces, are a kind of metasurface exploited mainly for WEH applications. Their objective is to extract as much energy as possible from as many as possible different kind of incident waves. Each signal has different incoming direction, polarization and frequency. Respect to rectifying antennas (RECTENNAs), the EM interaction between all the unit cells of the metasurface allows the structure to achieve the perfect absorbing property, therefore reducing the reflected portion of the incident wave, improving the quality of the system. Conventionally, to create a metasurface absorber structures, Split-Ring Resonators (SRRs) and Complementary Split-Ring Resonators (CSSRs) are commonly used. Depending on system requirements, different optimization can be designed (broadband, multiband, polarization insensitivity and wide-angle application).

"Focusing Metasurface", on the other hand, focuses the signal into a well defined point and direction. These kind of structures are usually realized thanks to phase-gradient metasurfaces (PGMS). This allows to modify the wavefront of the metasurfaces by changing the phase response of the signal once it goes through the MS itself, changing its direction. PGMS, based on the design, can obtain this in different ways offering different behaviors (see Fig.5):

1. focusing.
2. bending.

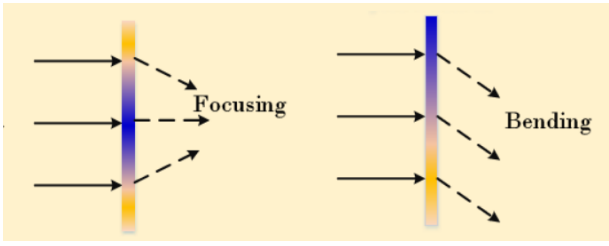

Figure 5: Visualization of the PGMS effects [3]

For both applications is present a change of the reflection and transmission behavior, violating the Snell's law. By utilizing an uniform phase variation, a bending effect can be obtained. On the other hand, if a variable phase distribution is exploited, it's possible to obtain a system that can concentrate into a well-defined point all signals regardless of theirs distance from the center of the structure. Therefore each

point of the metasurface points towards the same focusing region.

1.4 Metasurface for Absorption

Metasurface for absorption are a particular kind of metasurfaces used for WEH applications, their peculiarity is that the metasurface displays a resonance frequency in correspondence of which it behaves like a perfect absorber. Usually the most commonly used circuits are SRR and CSRR, but other circuits can be utilized. All of these allow the full structure to meet the criteria to be defined as metamaterial, if the metamaterial definition is not met the signals cannot propagate inside it and therefore cannot be absorbed.

With the objective of displaying the functioning behavior of absorber metasurface the following simulation has been reported. To reproduce the wanted behavior it's necessary to set up a periodic EM structure. The metamaterial shown in Fig 6 is considered. This metasurface has the goal of achieving a good performing MS that works with a wide incident angle and simultaneously reduce the complexity of the structure eliminating the previously introduced SRRs [4]. This metasurface, designed to work at 5.8

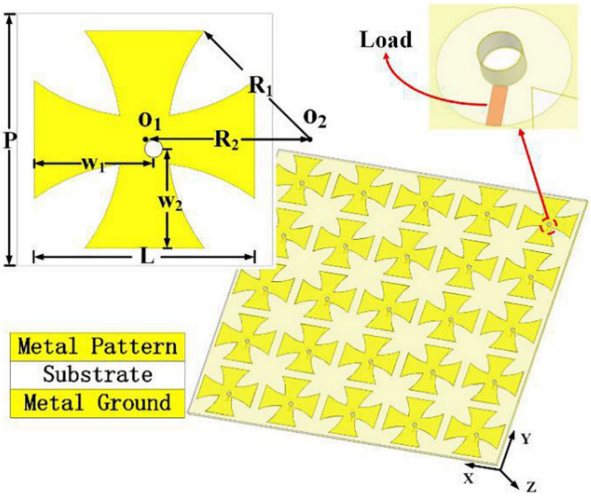

Figure 6: Metasurface absorber description [4]

GHz, is composed of 2 metallic layers separated by a PTFE substrate. The ground plane and the "*Celtic shaped cross*" are connected by a single via duct, and, between the pin and the ground plane, there's a variable load. The material used for the metallic part is copper with conductivity $\sigma = 5.8 * 10^7 S/m$, while the substrate has dielectric constant equal to 2.2 and $tan\delta = 0.001$.

All the copper layers have thickness m while for the PTFE substrate is h. The unit cell layout is displayed in Fig 6 where the following parameters are defined as: L the distance between the 2 opposite flat edges of the metallic layer ,W_1 and W_2 are respectively the distances between the center of the via duct and the left and bottom flat edge, R_2 is the distance at which the center of the circumference is placed away from the center of the unit cell and R_1 defines the radius of the arc on which the rounded edge it's built on. Each cell has length and width of P, the unitary cell is then repeated inside the full structure periodically. All the parameters are summed in the table 1. A simulation is set up on CST Microwave Studio environment that offers predefined template made specifically for the study of metamaterials, called *unit*

	m	h	L	W_1	W_2	R_1	R_2	P
Dimension [mm]	0.035	0.787	14.4	7.8	6.6	12	13.5	16.7

Table 1: Dimensions of the metasurface absorber

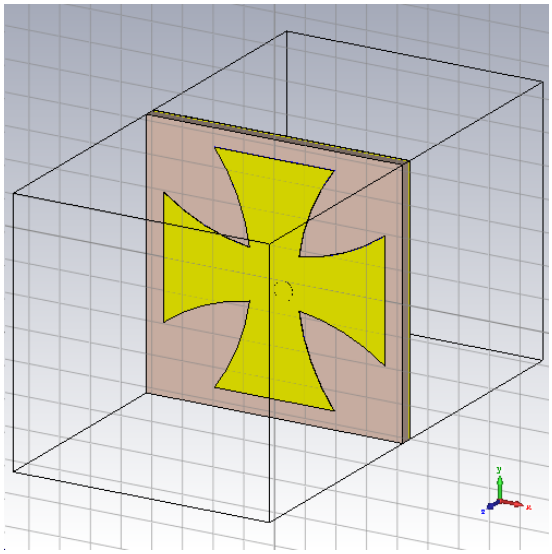

Figure 7: Front view of the model

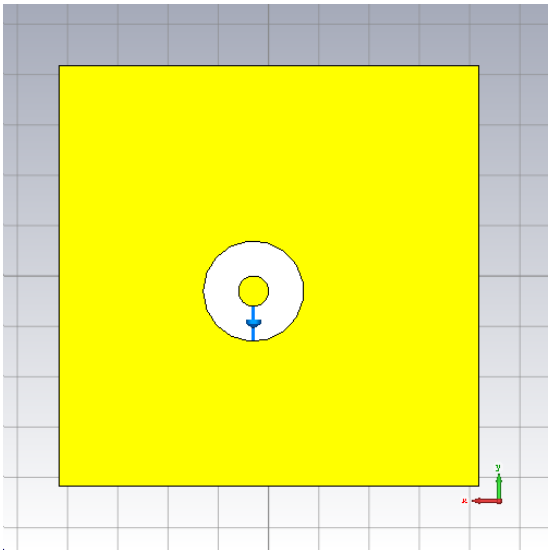

Figure 8: Back view of the model

cell. The procedure implies repeating the structure for each selected direction (in this case X and Y) such that we obtain an infinite array of identical unit cells. Thanks to this, the software takes into account the influence of adjacent cells without the need of designing the entire structure, reducing the design time. It is noteworthy to state that the simulation provided through this method is purely theoretical and ideal, since the software considers an infinite size metasurface, impossible to be realized. The *unit cell* template introduces 2 ports called "*Zmax*" and "*Zmin*". *Zmax* will be the port in the direction +Z, while *Zmin* in the direction -Z.

The simulation set-up can be observed in Fig.7 and Fig.8. The frequency range is between 4 and $6GHz$ and the engine is the so called "Frequency Domain Solver", more suitable for symmetric curved implementations. Moreover, a simulation varying the load impedance between 50Ω and 300Ω is provided thanks the "Parameter Sweep" tool. The simulated results are presented in Fig.9 and 10 where the values of ε and μ as function of frequency. As can be observed, in the frequency range the structure respects the operating principle introduced in this chapter, i.e. the permeability results to near zero while the permittivity much greater than 1, confirming the absorbing property already cited.

The absorbing nature can be verified also visualizing the S-parameters results, presented in Fig.11

In order to understand if there's a strong signal absorption by the structure it's expected to see a big spike in the in the interval around $5.8GHz$. As we can see we have a minimum in the S1,1 around 5.8 GHz, it represents that the signal doesn't get reflected by the surface and it is either absorbed by the structure or transmitted by it. In the meanwhile, the opposite happens for S2,1 where there's a maximum around the same frequency, which corresponds to an higher transmission level of the signal through the

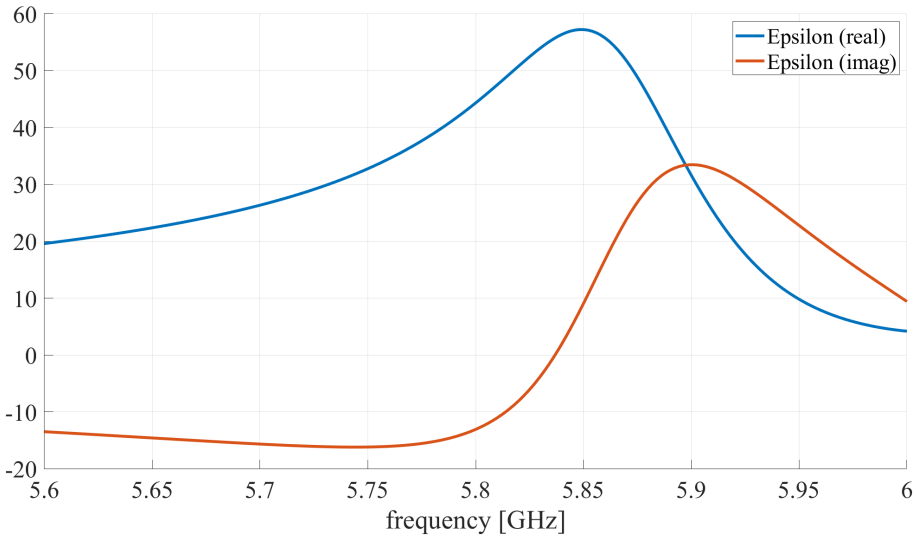

Figure 9: ε of the material

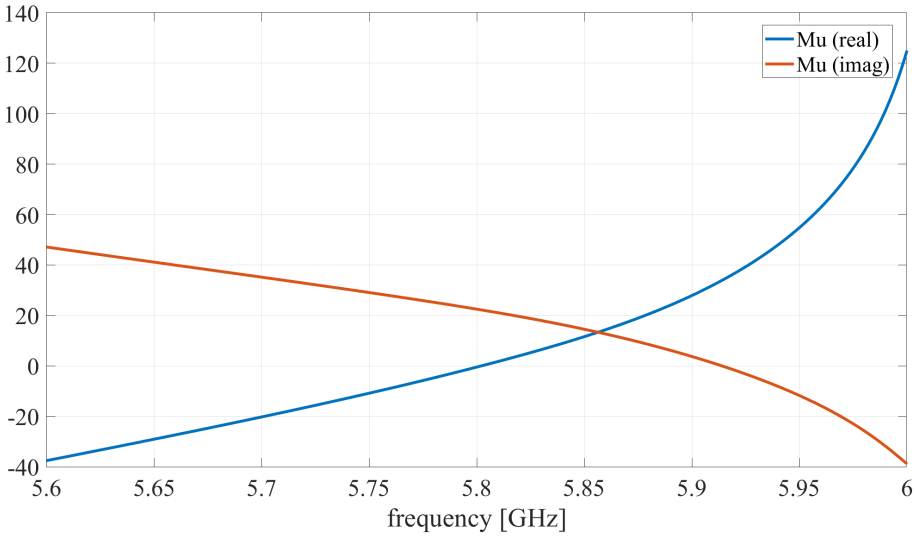

Figure 10: μ of the material

material. Since the transmittance level is still quite low (around $-17dB$) it means that the signal can pass better through the surface than other frequencies. By analyzing the formula of absorbed power: $A = 1 - S_{1,1}^2 - S_{2,1}^2$ it's possible to find that at around 5.8 GHz the absorbance level is 99.87%, therefore the signal is almost completely absorbed by the structure.

Finally, the simulated results varying the impedance of the load are presented in Fig12, where current flowing trough the load is figured as function of frequency. As it has been anticipated before, the simulation needs be to performed with different load values to better understand which load is results the optimal choice in terms of energy absorption. The value of 50 Ohm represents the best choice, confirming what has been found in [4].

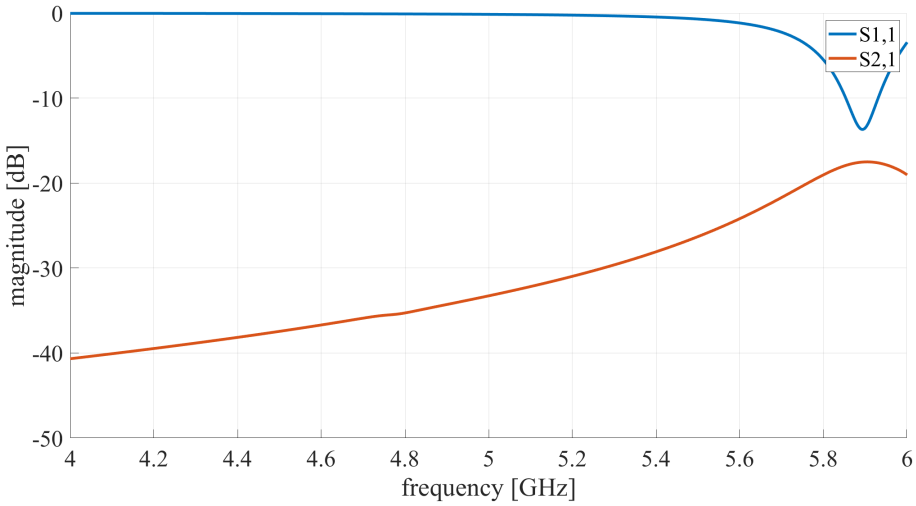

Figure 11: S-parameters of the absorber

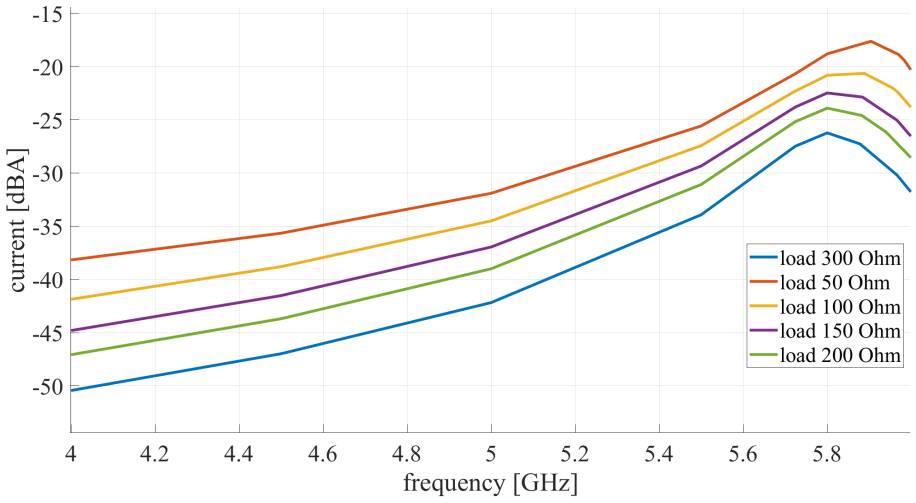

Figure 12: Current through the lumped element with different loads

1.5 Metasurface for focusing

In this section is presented the design of a metasurface able to focus energy into a well defined region of space, exploiting therefore the ranging capability, real objective of this thesis work.

In literature, the most known technique exploited for focusing is the one that implies metasurfaces called Phase-Gradient Metasurfaces (PGSM). They present the ability to exploit the phase-shift created by each element such that the interaction between elements changes the wavefront direction. Afterwards, the objective is to design the wavefront such that the transmitted wave will point towards the same point, that from now on it will be referred as "focus".

As a starting point for designing focusing metasurfaces for powering application, the structure operating at 10 GHz proposed in [5] has been analyzed. This work introduces a phase gradient metasurface that focuses the signal into a region after it, independently from the angle of arrival. To design this metasurface it's required to analyze different unit cell element designs along with their phase-shift response. It is relevant that the transmittance levels of each design has to be as high as possible in order to create an uniform wavefront.

The metasurface is composed of 2 metallic layers realized in copper, separated by a substrate "*Rogers F4B220*" with permittivity $\varepsilon_r = 2.2$, loss $tan\delta = 0.008$ and thickness is $h = 2.5$ mm. The substrate length and width is $p = 11.5$ mm, $w = 1$ mm, $g = 1.5$ mm, $\alpha = 150°$ and inner radii vary from 0.1 mm to 1.84 mm. as shown in Fig.13.

Given the operating frequency and the desired focusing distance, it is possible to easily retrieve the

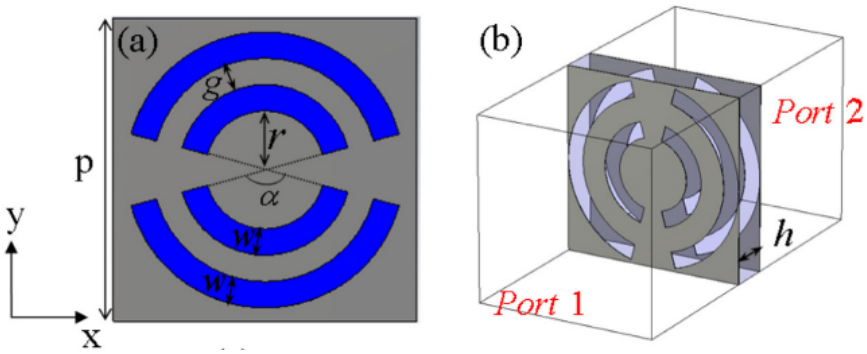

Figure 13: Model used for the PGSM metasurface [5]

phase distribution of the wavefront through a derived version of the Snell's Law, expressed as:

$$\phi(x) = \frac{2\pi}{\lambda}(\sqrt{(x - x_0)^2 + F^2} - sin(\theta_i * x)) - \frac{2\pi}{\lambda}F + \phi_0$$

λ represents the wavelength of the signal, F is the focal length and ϕ_0 is the center phase. If metasurface is thought to operate at different origins and therefore directions multiple test on θ_i must be considered, that represents the incident angle from which the wave hits the metasurface, and x_0 , which symbolize the distance between the focus and the metasurface's center projected on a plane at distance F from the surface itself. In most applications x_0 and θ_i are usually kept equal to 0, therefore only waves perpendicular to the MS are considered to compute the phase distribution and the focus point is on the

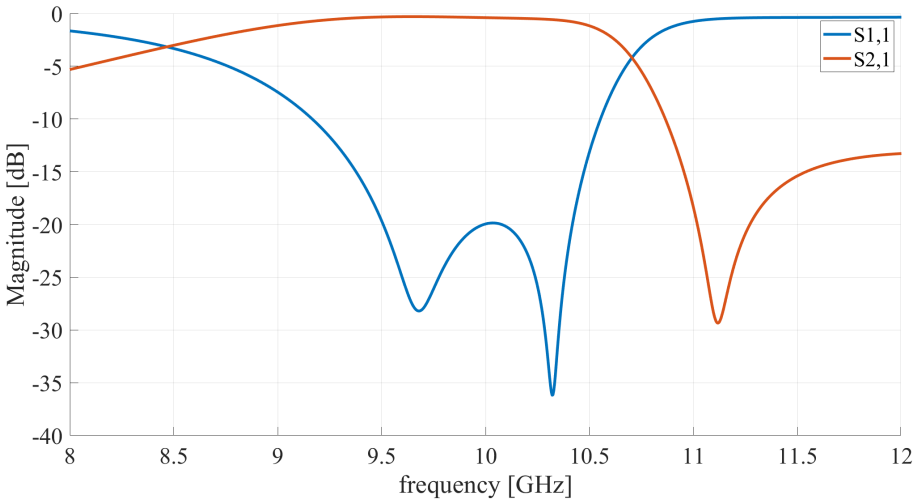

Figure 14: S parameters of the unit cell element with r = 1.84 mm

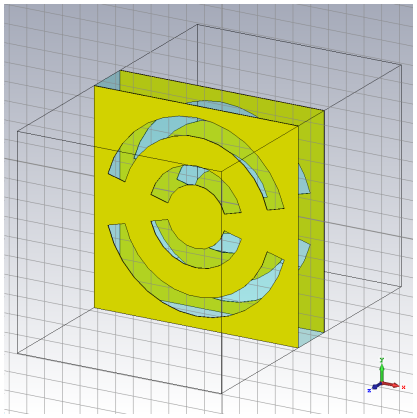

Figure 15: PGMS unit cell

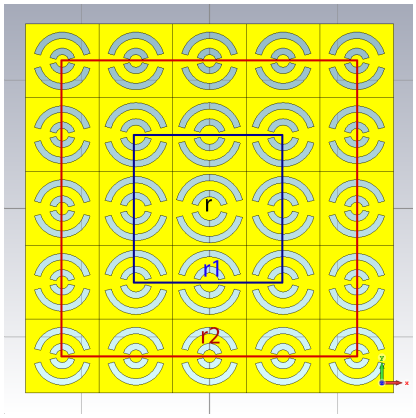

Figure 16: Simulated PGMS full structure

same point of the structure's center projection. $\phi(x)$ represents the phase distribution of the wavefront with respect with its coordinate system. Therefore, by knowing the focal length (F) and the frequency of the signal (f) it's possible to compute phase-shift introduced by each unit cell.

In Fig.15 it's represented the unit cell model in the CST environment. By varying the inner radius r the phase shift can be obtained by checking the phase of the S-parameters obtained by the simulation. In particular we are interested on the transmitted signal's phase, therefore the phase of S2,1 it's analyzed. Before building the full metasurface model, it's necessary to check if the MS works properly around 10 GHz. In figure 14 the S-parameters given by the unit celll simulation on CST are presented, showing an high level of transmitted signal (S2,1) and at the same time a low level of reflected signal (S1,1) in range of frequency between 9.5 and 10.5 GHz. Finally, a 5x5 matrix (differently from [5]) is designed and shown in Fig.16, grouping different unit cells to form a concentric structure with the following values: $r = 1.84$ mm, $r_1 = 1.5$ mm and $r_2 = 1$ mm. The radius value is responsible of the phase shift of each rings. The main element is the unit cell with inner radius $r = 1.84$mm and its phase shift value is taken as reference. Therefore, for the unit cells with inner radius equal $r1$ and $r2$ the phase shift is computed as the difference between the transmitted signal phase found in S-parameters on CST and main element phase. The graph in Fig.17 shows the phase shift as function of the inner radius value at 10 GHz. The

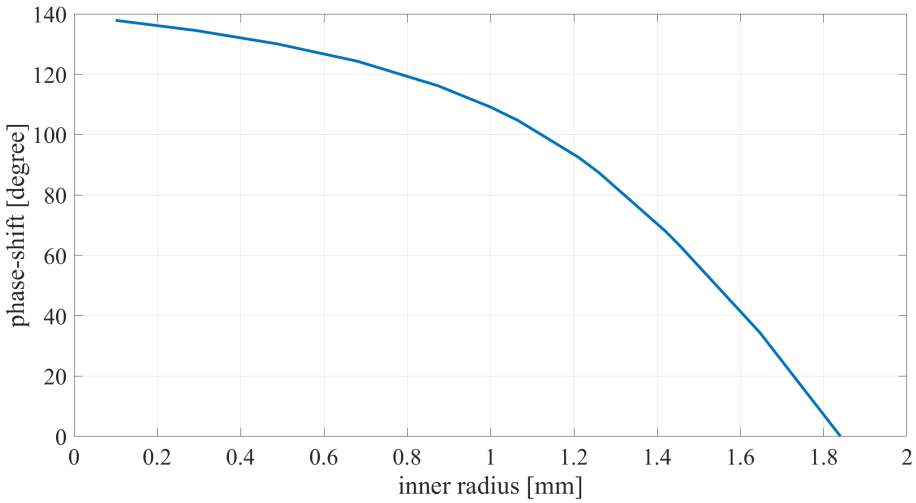

Figure 17: Phase-shift of each unit cell by varying the inner radius r at 5.8 GHz

phase shift obtained for $r_1 = 1.5$mm and $r_2 = 1$mm are respectively 57 and 109 degrees.

Therefore, the full surface presents approximately 50/60 degree of phase shift between each ring. To verify if the structure actually focuses the incident wave into a confined region we have to introduce a plane wave element that results x-polarized with $1V/m$ field intensity and it propagates in the $-Z$ direction, perfectly perpendicular to the surface. The field has been computed up to 300 mm away from the metasurface itself and the results are presented in Fig.18, showing a focusing point at around 200 mm from the surface.

In order to understand the focusing quality, the figure of merit of the beam collection efficiency (BCE) is introduced, representing the ratio between the energy around a predefined portion of plane and the energy spread over the entire surface containing the interested plane, described by:

$$BCE = \frac{\int_S P(S)\, dS}{\int_{S_{tot}} P(S)\, dS}$$

The BCE is used to define the metasurface efficiency at focusing the energy into a predefined area, therefore giving the designer an idea on its performance. The BCE is computed over a considered area of 576 mm^2 and compared to the overall available area of 3306 mm^2. The results are presented in Fig. 19, It can be seen that 28% of the power is concentrated inside the considered area. As example, if a rectenna is placed in this region, it would be able to capture up to 28% of the total available power and this represents a good starting point for designing efficient focusing MS.

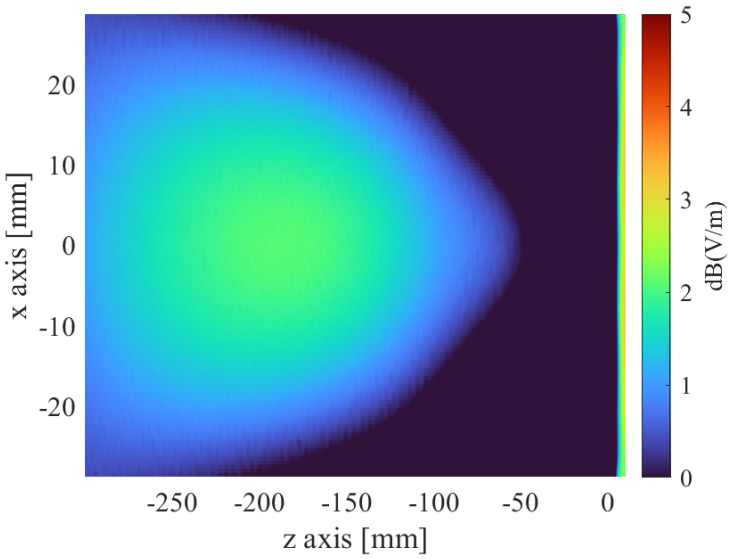

Figure 18: Display of the Near-field excited by the metasurface

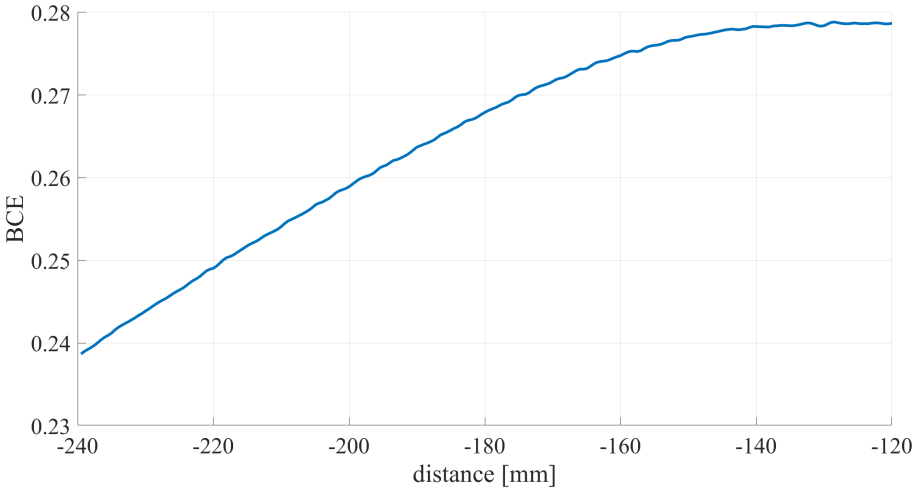

Figure 19: BCE computation over the surface

2 Designing a new metasurface for focusing applications

2.1 Adapting the metasurface for focusing application

In this chapter the design of a proper metasurface for WPT/WEH application is presented. As a starting point, it's explored the feasibility of adapting the previously introduced absorber metasurface, taken from the article [4] and presented in section 1.4, into a focusing metasurface, considering as unit cell the " *Celtic cross*" design, as shown in Fig. 20, modifying its structure and then designing a concentric topology for making it feasible for ranging applications, as shown in Fig.21.

Aim of this work is to design a PGMS able to enhance transmission of EM power and reducing as much as possible any kind of reflection and absorption created by the structure, obtaining the minimum energy loss at the receiving end of the system. In order to accomplish this, it's mandatory that the ground plane, the via duct connecting the 2 metallic layers, as well as the variable load, must be removed. Starting with the dimensions described in the chapter 1.4, the new unit cell is simulated to retrieve its frequency response and therefore computing its operating bandwidth. From Fig.22, showing respectively

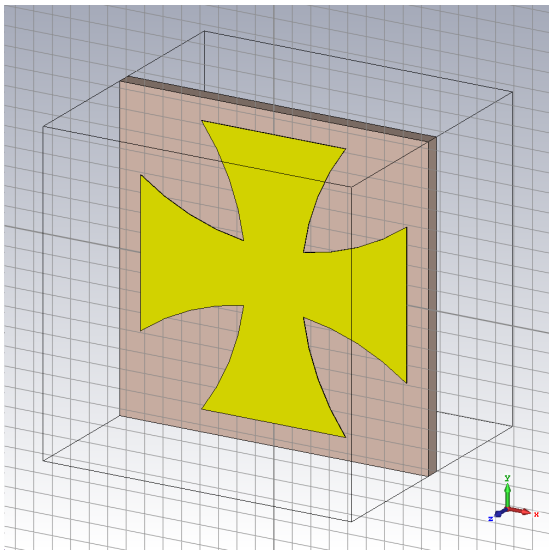

Figure 20: View of the unit cell model

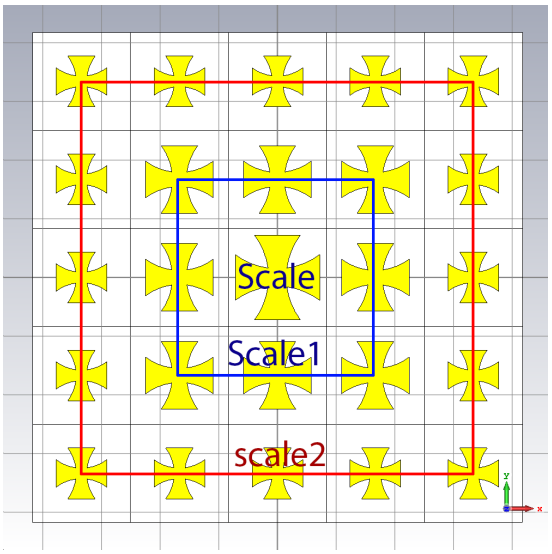

Figure 21: View of the full surface

S1,1 and S2,1 of the unit cell, it's possible to extract the operating frequency which corresponds at $12.6GHz$. This unit cell represents the central element and will be used as reference for designing the full structure presented in figure Fig.21. In order to design it, it is mandatory to obtain information about the phase shift introduced by surrounding elements. Following the procedure illustrated in the chapter 1.5, simulations of the single unit cell changing its dimension has been performed. Keeping constant the substrate thickness, the size of the "Celtic Cross" has been linearly scaled by a factor that ranges from 1 to 0.5. For each condition the phase of S2,1 has been obtained and compared with the phase of central reference element (that corresponds to a scale factor equal to 1). The results are presented in fig.23.

Once obtained the behavior of every single unit cell it's possible to design the full metasurface structure. The final design foresee 5x5 matrix composed of 3 rings with different scale factors. Based on the phase shifts presented previously, several design have been simulated. They differ one each other depending on

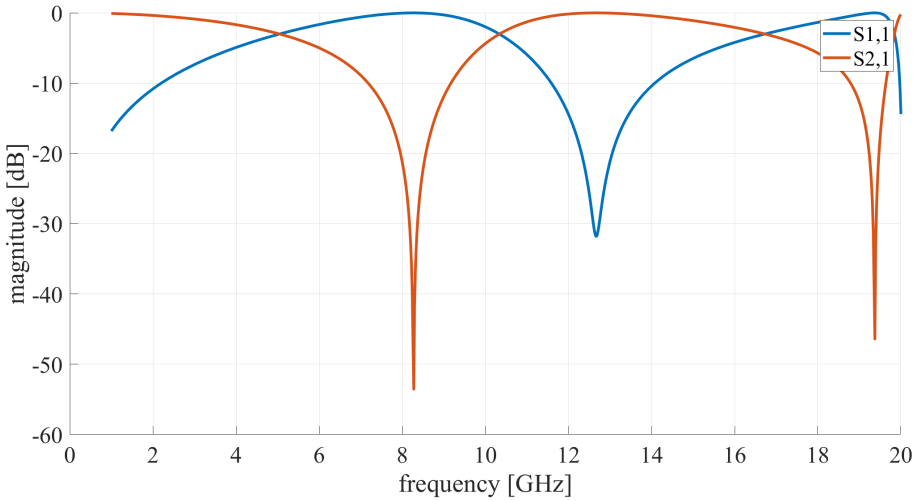

Figure 22: Unit cell S-parameters

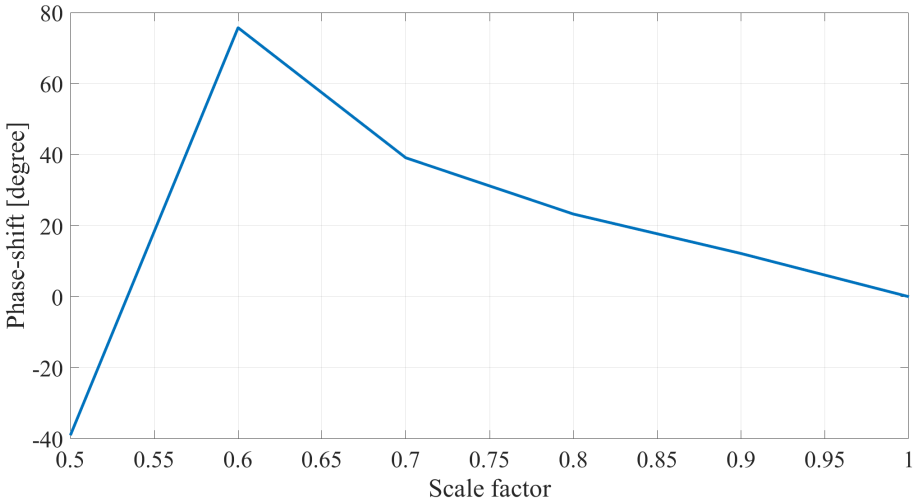

Figure 23: Phase-shift of each unit cell by varying the scale at 12.6 GHz

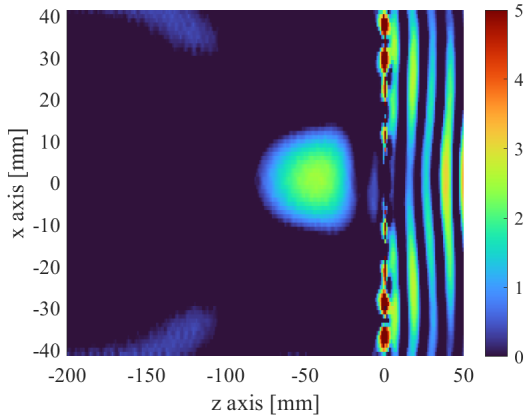

Figure 24: (0.6, 0.8, 1) full metasurface field

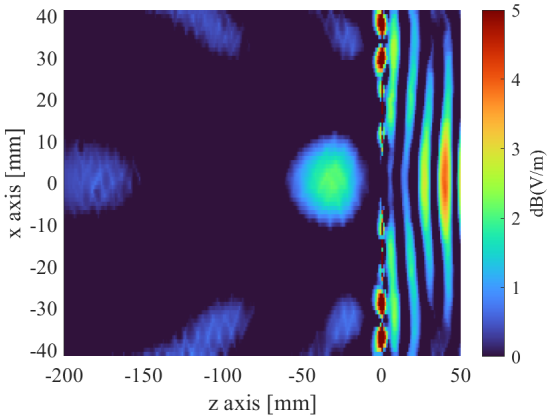

Figure 25: (0.5, 0.75, 1) full metasurface field

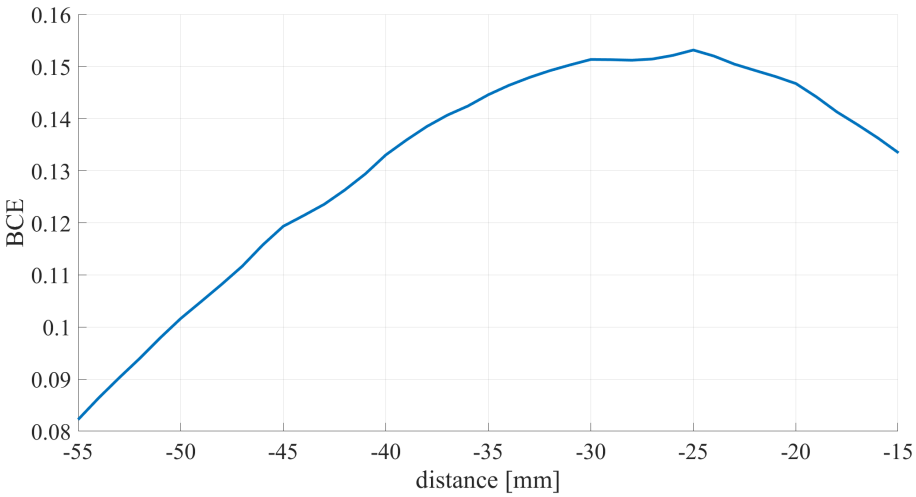

Figure 26: BCE computation of (0.5,0.75,1) model

the scale factor used and they will be referred with the nomenclature $(scale2, scale1, scale)$, as shown in Fig.21, where *scale2* and *scale1* represent the scaling factor of the third and second outer ring, respectively, while *scale* represent the scaling factor of the main element, that is always equal to 1, being the reference. The fields are extracted by inserting a probe at (0,0,-200) while the metasurface is excited by a plane wave propagating in the $-Z$ direction. Among all the simulations, the most promising results are provided by $(0.5, 0.75, 1)$ and $(0.6, 0.8, 1)$ combinations, showing the highest field intensity and levels of BCE, illustrated in figure 24 and 25.

As it can be evinced, the metasurfaces, placed at exactly on the origin of the Z-axis, generates a focusing effect in the same region, practically. In particular a peak it's present at -44mm for (0.6,0.8,1) and -32mm for (0.5,0.75,1) with respectively $1.74V/m$ and $1.66V/m$.

On the other hand, in order to evaluate correctly the focusing performance, the BCE must be computed. For (0.5, 0.75, 1) the considered area is 529 mm^2, instead for (0.6, 0.8, 1) the surface is equal to 729 mm^2 both compared to the overall available area of 6889 mm^2. The results are shown in Fig.26 and 27. The BCE graph shows that (0.6,0.8,1) focuses the most power at around -36 mm, close to the maximum intensity peak shown before, while (0.5,0,75,1) is at -25mm. In this case, BCE also represents how much power is dispersed outside the focusing area, therefore the higher the value the less energy has

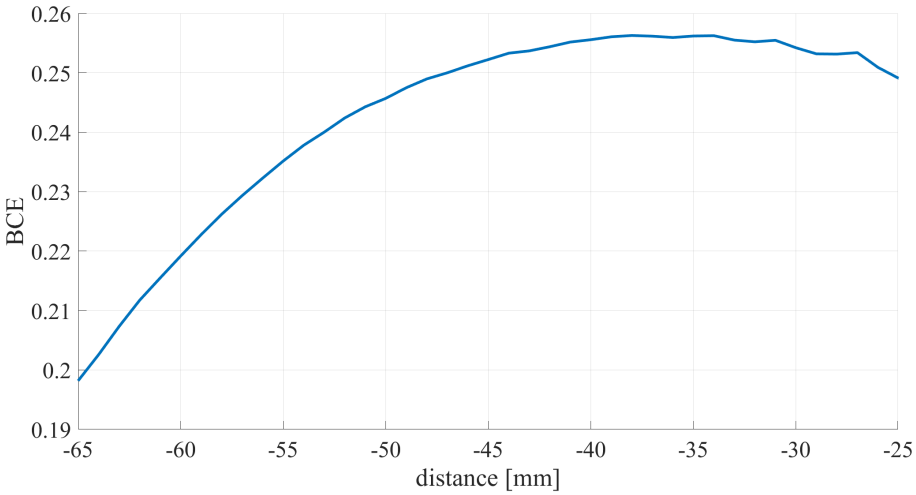

Figure 27: BCE computation of (0.6,0.8,1) model

been wasted. To summarize the results of the models are shown in table2.

As a conclusion, it can be evinced that (0.6,0.8,1) combination represents the most efficient one for focusing energy closer to the focal point, with more than one forth of the total available power confined around it.

	(0.6,0.8,1) model	(0.5,0.75,1) model
Peak power [V/m]	1.74	1.66
Peak power distance [mm]	-44	-32
Max BCE	0.255	0.152
Max BCE distance [mm]	-36	-25

Table 2: Comparison of the received power

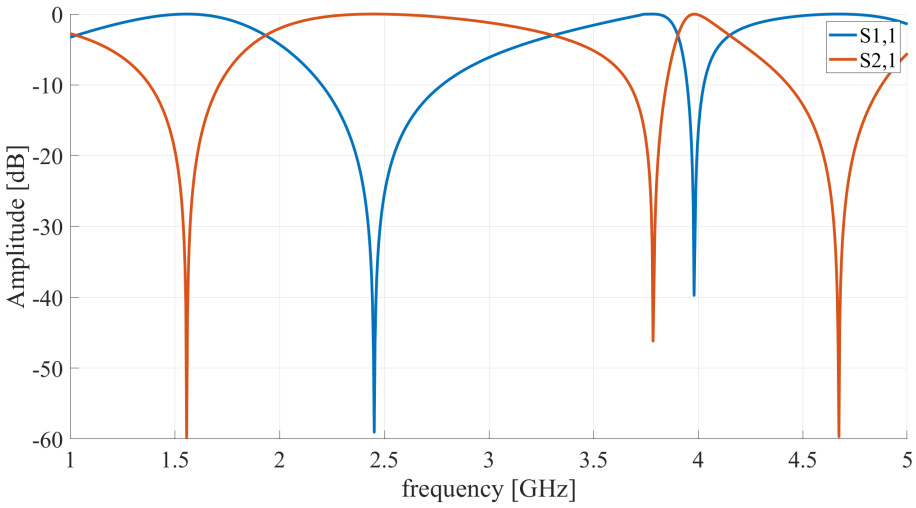

Figure 28: S-parameters of the main element

2.2 Adapting the metasurface to work at 2.45 GHz

Considering the presented design, it's now possible to change the structure behavior in order to change its working frequency at 2.45 GHz, the target operating frequency chosen for the final project, since in this band is possible to harvest excellent amount of power since it is unlicensed and broadly utilized. In order to change the working frequency of the unit cell element it's necessary to enlarge the overall size of the main element. It can be found that the overall size is approximately 5.68 times larger than the one displayed in the chapter 1.4. Therefore referring Fig.6 the dimension become the followings: $R_1 = 68.16$mm, $R_2 = 76.68$mm, $L = 81.792$mm, $P = 94.856$. Therefore the change of frequency is strictly connected to dimension of the structure, allowing to design other structures working at different frequencies, if needed.

As show in Figure 28 the new unit cell presents a minimum of reflection and a maximum of transmission coefficient at 2.45 GHz.

As previously illustrated, once the working frequency has been fixed, it's possible to design each single unit cell element trying to find correct phase shift in the transmitted wave signal respect to the reference element. With the same procedure, a scaling factor ranging from 1 to 0.2 is applied. The results are shown in Fig.29, from where can be evinced that by changing the scaling factor the phase changes accordingly. The same nomenclature adopted previously is retrieved.

After testing different combinations the 5x5 full surface that showed the most promising result was $(0.56, 0.84, 1)$, with a total dimension of 474.28 mm x 474.28 mm, shown in Fig.30, while its field in Fig.31. The metasurface's properties are analyzed by emitting a x-polarized plane wave with $1V/m$. From figure 31 maximum peak field intensity of $1.58V/m$ at 250 mm away from the full structure can be noted. Moreover, the BCE is also computed to effectively demonstrates its focusing capability and results are presented in Fig. 32. The BCE has been evaluated over a considered area of 22 500 mm^2 and has been compared to the overall plane of size 224 676 mm^2. It can be evinced the focal point is around -215 mm, where almost 1/5 of the total transmitted power is concentrated.

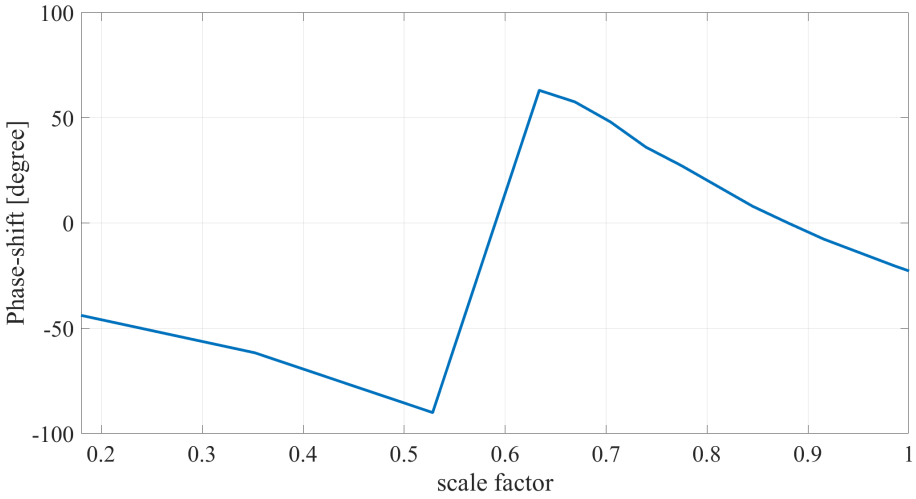

Figure 29: Phase shìft by changing the scaling factor at 2.45 GHz

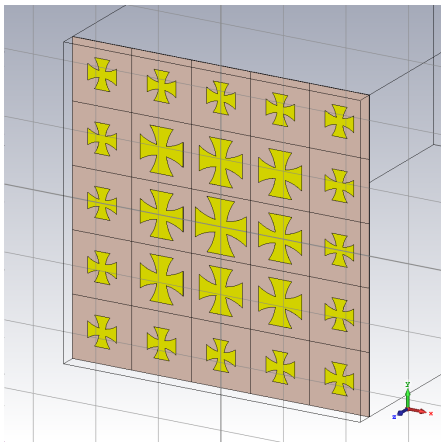

Figure 30: Full surface model

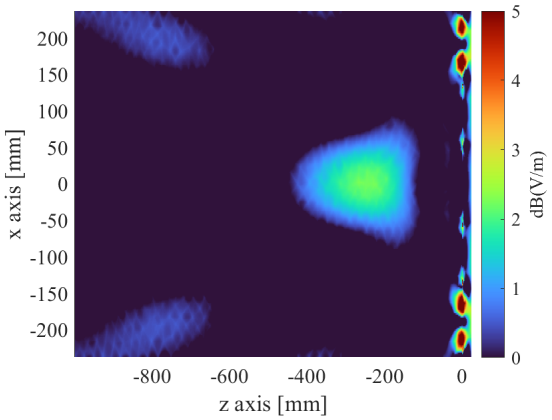

Figure 31: Full surface field representation

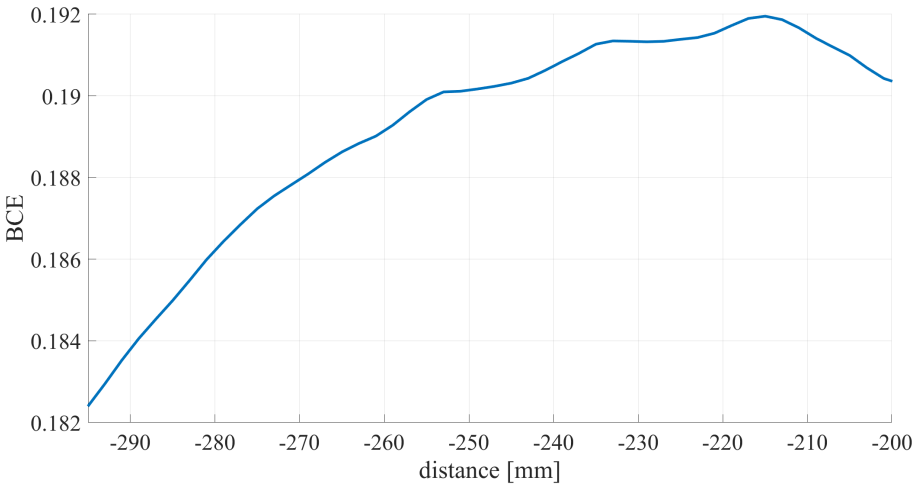

Figure 32: Full surface BCE

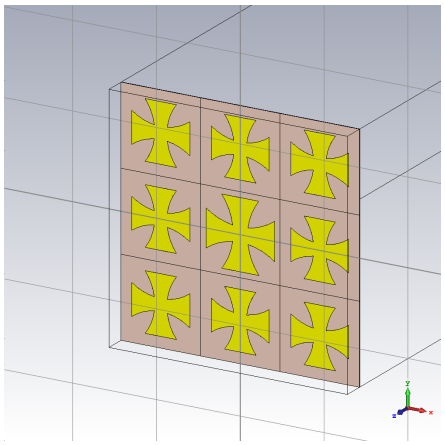

Figure 33: 2 ring model

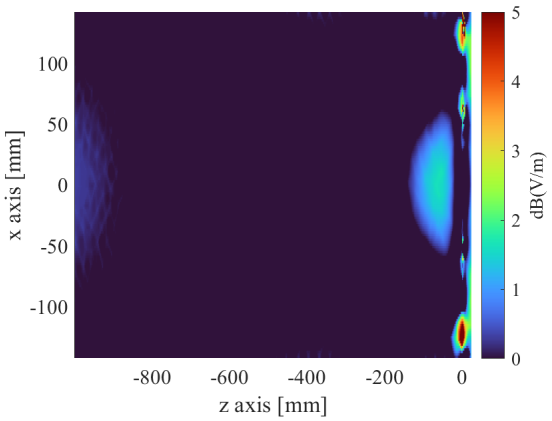

Figure 34: Field intensity of the 2 ring model

2.3 Creating a smaller model

The design presented in the previous section composed by the 3 concentric rings offers excellent focusing performance. On the other hand, scaling the frequency at 2.45 GHz has required to increase the size of the overall metasurface. In order to reduce the space consumption, in this section a compact solution is proposed. Respect to the design of section **??**, a more compact design of the metasurface is proposed by removing the more external ring. The novelty stands in the removal of the outer rings, Using the same nomenclature introduced previously, the new topology will be referred as $(-, 0.84, 1)$ and is presented shown in Fig.33.

To better distinguish the 2 model this new metasurface will be called as "*2 ring model*" while the structure from which it is inspired by will be called "*Full surface model*". This structure presents a width and height of 284.57mm, ensuring a 40% reduction in dimension respect to the previous one.

Again, the excitation through a plane wave propagating in negative z direction is performed. The field, showed in Fig.34 displays a maximum peak at -62mm from the surface with $1.42V/m$ of field intensity. The most interesting property is that its focusing point is much closer to the surface itself, allowing to collocate the metasurface much closer to the receiving antenna compared to the case of the full surface, with the drawback of decreased maximum intensity. The BCE is computed considering an area of 10 816 mm^2 respect to a total surface of 80 656 mm^2 . The results are shown in Fig.35 for different distances from the metasurface. It can be noted that is present a maximum of power focused around the focal point at -53mm with more than the 26% of total power stored in the considered surface. In conclusion, the new structure focuses less power respect to before but offers an easy implementation for its geometric constrains, allowing to offer a more compact solution.

The comparison in terms of maximum intensity and BCE is summarized in table 3.

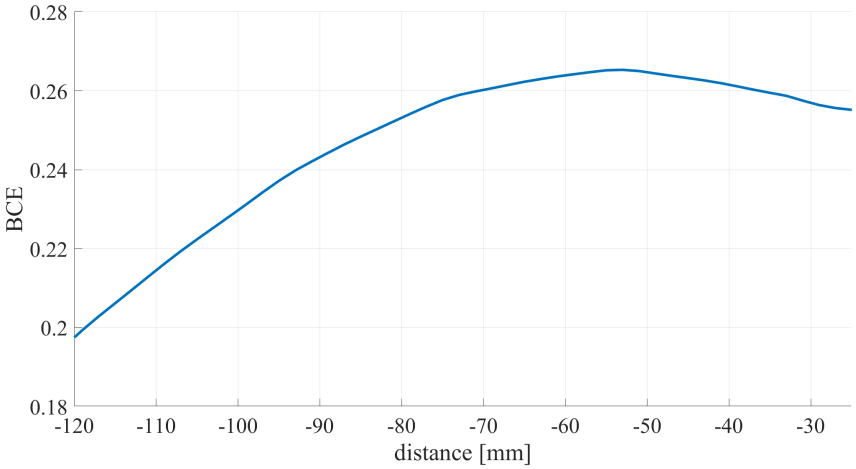

Figure 35: BCE of the 2 ring model

	Full surface model	2 ring model
Peak power [V/m]	1.58	1.42
Peak power distance [mm]	-250	-62
Max BCE	0.192	0.265
Max BCE distance [mm]	-220	-25

Table 3: Comparison of the received power

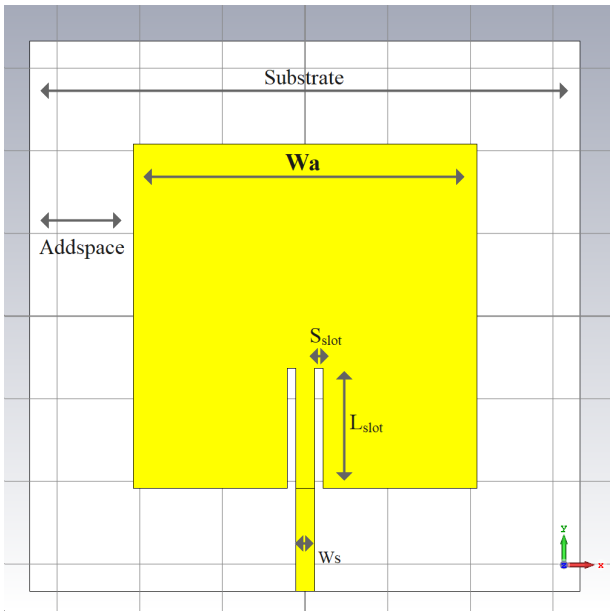

Figure 36: Patch antenna model

3 System simulation and result validation

3.1 Patch antenna design

To verify if the metasurfaces presented in the chapter 2 actually work, a reference antenna has to be considered and designed. The antenna will be the element before the rectifier, therefore responsible of capturing the field focused by the metasurface. At the same time, it can be considered as transmitting element, recreating a more realistic environment replacing the plane wave excitation.

As radiating element is considered a patch antenna, realized in planar technology that offers good performance in terms of gain and directivity in a compact and low-cost design.

The design is presented in 36. The metallic layers are realized in a 0.035 mm copper, while as a substrate has been used PTFE of thickness 0.787 mm ($\varepsilon = 2.1$, $tan\delta = 0.0002$). The feeding line is realized in coplanar microstrip edge with inset technique and its width is computed in order to obtain 50.54Ω as input impedance, value confirmed by the waveguide port impedence calculator of CST. The choice of 50.54Ω is a common choice in RF design, since most used connectors present this value as input impedance. In order to resonates at the the frequency of 2.45 GHz, a tuning of the patch length (and width, since it is a square patch) for centering the resonance and the inset for matching it has been performed in CST. Finally, the ground plane, realized in copper, presents the same dimension of the substrate. All the dimensions are reported in the table 4.

	metal	*h*	W_A	W_S	*Addspace*	*Substrate*	L_{slot}	W_{slot}
Dimension [mm]	0.035	0.787	41.5	2.3	12.5	66.5	14.5	66.5

Table 4: Dimensions of the antenna

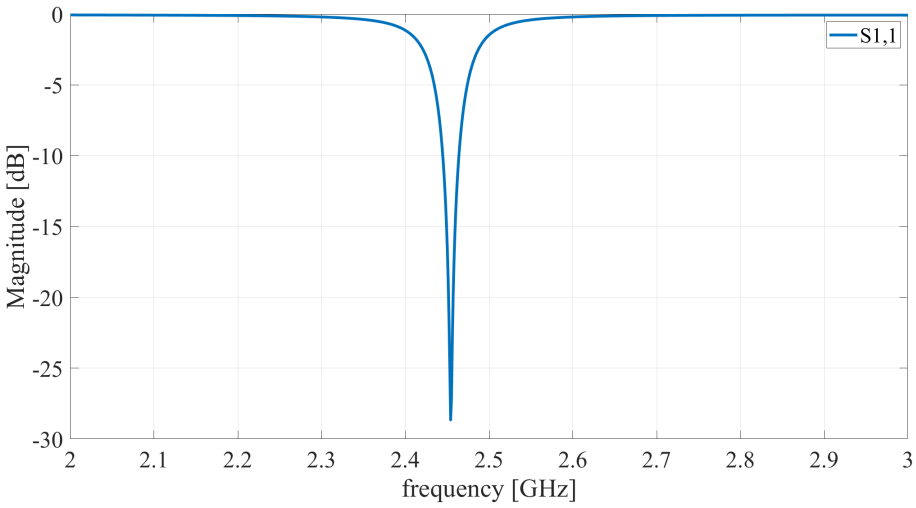

Figure 37: S1,1 of the patch antenna

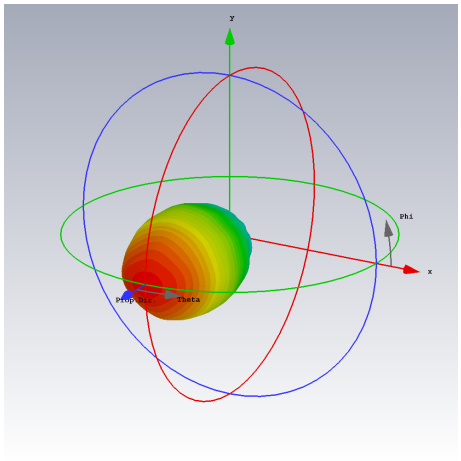

Figure 38: Far field antenna gain

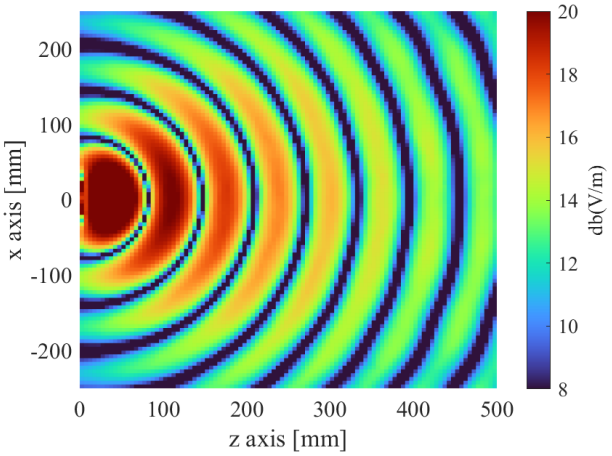

Figure 39: Wavefront generated by the patch antenna

As shown in the S-parameters graph in Fig.37, the square patch presents a bandwidth that ranges from 2.444 to 2.646 GHz and a gain of the antenna is $6.942dB$, whose pattern is presented in fig. 38. For comparison with the next simulations, in Fig.39 is shown the wavefront and field intensity generated by the antenna at a fixed time instant. The antenna has been simulated considering a bounding box of 250 mm in both positive and negative X and Y direction and 500 mm in positive Z direction. This step is necessary in order to have the same considered area to compare the patch antenna with other simulations that will be taken in a later moment. It's noteworthy that the field at 500mm from the patch antenna is not completely in far-field area and therefore the field can not be considered as ideal plane wave.

	Only patch antenna	Patch and 2 ring model	Patch and full surface model
W_A [mm]	41.5	41.3	41

Table 5: Dimensions of the antenna parameter based on the simulation

3.2 Antenna and metasurface simulation

Once the antenna has been designed it's now possible to verify the effect of the metasurfaces on a wireless link. The patch antenna is used as transmitter in this first stage. The simulations that has been set up analyze three different scenarios: the first one regards the case where the metasurface is not involved, therefore only the patch is considered and it will be referred as "only patch antenna". The second is the one involving the 2 ring model metasurface in front of the radiating patches, called "Patch and 2 ring model", and finally the one involving the full surface model metasurfaces, called "Patch and full surface model". For the first case the field has been already presented in the previous section, instead the other two scenarios are presented in the following.

It is need to be stated that the presence of the metasurfaces in the proximity of the patches has required to slightly tune the antennas' dimensions due to their interaction, as reported in table 5. The field generated by the "Patch and full surface model" can then be seen in Fig.40 and with zoom out in Fig.41. On the other hand, the "patch with 2 ring model" results are presented in figure 42 and its zoom out in figure 43.

By comparing the fields generated by the patch antenna in presence and absence of the metasurface it can be noted a quite noticeable difference. In fact, without the metasurface the highest dynamic E-field registered by CST is -67dB at 500 mm from the antenna itself, while in the systems involving the 2 ring model and the full surface model are respectively -64dB and -62dB, at the same distance. It can be noted also an unwanted effect of the metasurface, i.e. the formation of secondary beams propagating in several directions.

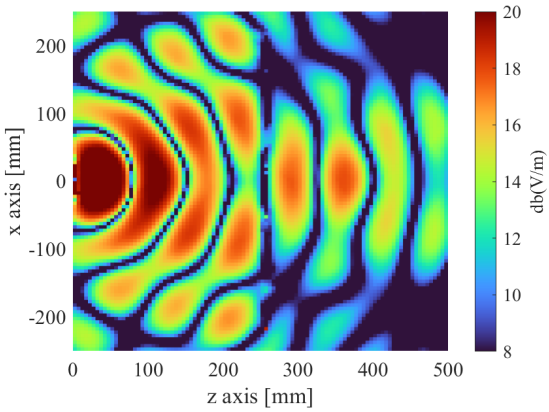

Figure 40: Field of the patch antenna with the full surface model as a radome

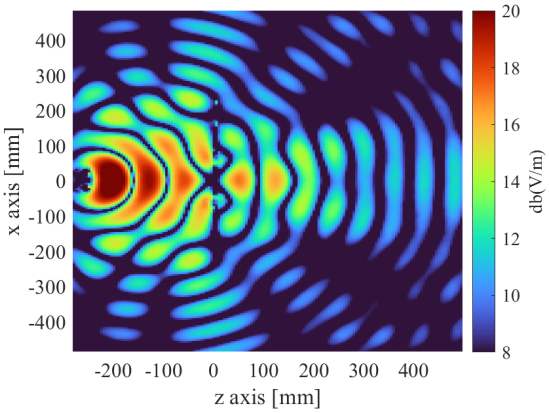

Figure 41: Wider angle of the patch antenna and full surface model

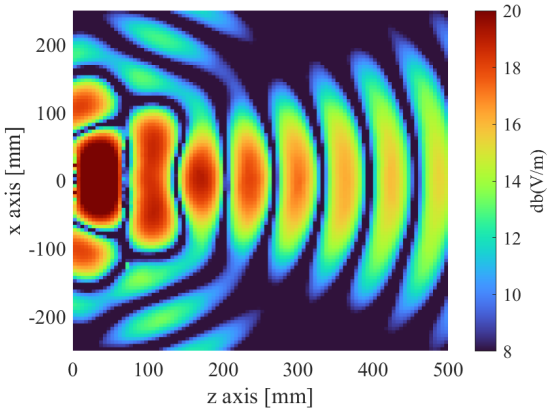

Figure 42: Field of the patch antenna with the 2 ring model as a radome

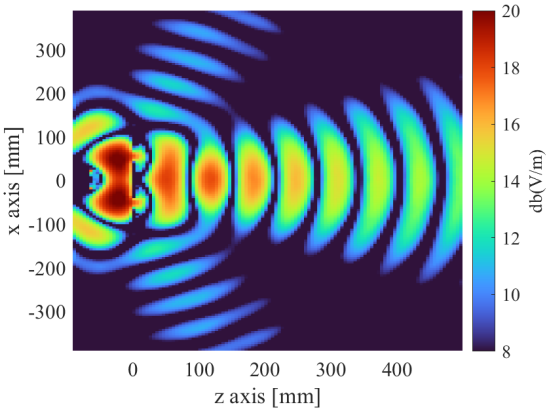

Figure 43: Wider angle of the patch antenna and 2 ring model

3.3 Power budget computations and results validation

To validate the functionality and the deployability of the system, it's necessary to set up a simulation where both the transmitter and the receiver are present and exchange power. Therefore the 2 patch antenna are deployed at 1000 mm apart the metasurfaces will be included between the 2 patch to, hopefully, increase the overall efficiency of the harvested energy by the rectifier antenna.
Since, as stated in principle, the link distance and the antennas' dimensions does not fit with the far field condition, it is not possible to retrieve the Friis formula:

$$\frac{P_r}{P_t} = G_t G_r \left(\frac{\lambda}{4\pi R}\right)^2$$

Since the condition $R >> \lambda$ is not completely met, the system propagates in the radiative near-field region instead of the far-field region. In the radiative near-field there could be some reflections created by the receiving antenna that might cause some distortions and therefore degrade the received signal strength.
To obtain more precise results the methodology described in the article [6] is utilized. In the article is introduced a Matlab simulation process to compute the received power by exploiting the equivalence and reciprocity theorem.

$$\int \mathbf{J}_1 \cdot \mathbf{E}_2 \, \mathrm{d}V = \int \mathbf{E}_1 \cdot \mathbf{J}_2 \, \mathrm{d}V \ .$$

The reciprocity theorem implies that antennas work equally well as transmitters or receivers, and specifically that an antenna's radiation and receiving patterns are identical.
The algorithm to function requires the 3D e-field and h-field imported by CST over an area spanning $(Xmin, Xmax, Ymin, Ymax, Zmin, Zmax)$ of $(-250, 250, -250, 250, 0, 500)$mm that corresponds to the area shown in the figures 39,40,42. It then computes the equivalent fields: E_S,H_S,E_H and H_H. E_S and H_S are the equivalent fields for the source antenna, while E_H and H_H are the equivalent field for the receiving antenna placed at 500 mm from the patch antenna. Therefore by plugging the field into the Matlab code the model of the receiver and transmitting antenna are computed and they describe how the field behaves at that distance.
The equivalence fields are obtained by utilizing the equivalence theorem where the equivalent current are obtained.

$$J_s = \hat{n} \times (H_1 - H); M_s = -\hat{n} \times (E_1 - E)$$

These 2 imaginary surface currents (J_s, M_s) represent the field over a defined surface outside the volume occupied from the physical antenna, in this case over the $Z = 500$mm XY-plane, this new source generates the same identical field as it was the original antenna, hence equivalent. It's now necessary to compute the field for each single simulation, in particular are required the "only patch antenna system" and "patch and metasurface system" (for both the 2 ring and full surface models). From the only patch system it's necessary to obtain both (E_S, H_S) and (E_H, H_H) fields, since the patch will be used both as transmitter and receiver, while for the patch and metasurface system only (E_H, H_H) is required. Since every simulation take place at 500mm away from the patch antennas the 2 distances add up, resulting

in 1m of total distance. By comparing the equivalence fields of the source and receiver it's possible to compute the surface current at the other end, from which is possible to compute the received power.
Three simulations can now be set up:

1. 2 patch antennas looking at each other 1 meter apart.
2. A patch antenna looking at the 2 ring model with the receiving patch antenna at 66 mm from the metasurface itself.
3. A patch antenna looking at the full surface model with the receiving patch antenna at 253 mm from the metasurface itself.

	Patch to Patch	Patch to *2 ring model*	Patch to *full surface model*
Current I $[A]$	$-0.01945 - i2.507 * 10^{-5}$	$-0.02398 - i0.00093$	$-0.04144 + i0.00064$
Current magnitude I $[A]$	1,945E-02	2,399E-02	4,145E-02
Rx Power P_r [dBm]	**-13.3**	**-11.4**	**-6.7**

Table 6: Comparison of the received power

The results obtained by the simulator and can be shown in table 6. The results show how strong impact the full surface model has in comparison to the 2 ring model and in absence of any metasurface to enhance the signal strength. In fact, there's an increase of 6.6 dB, corresponding to an increment of 4.57 times compared to not having any metasurface.
For checking the received power results, a simulation with 2 patches at 1 meter of distance has been performed directly on CST. Only one of the antenna is stimulated by a port while the antenna is completely passive and it's used as a probe to check the signal strength and received power. This can be evaluated through the S-parameters, shown in figure 44 . Due to the 2 patches being in the radiative near-field the working frequency of the excited patch antenna slightly changes, but 2.45 GHz it's still well within the working frequency range. In the simulation the maximum excited power is at 2.42 GHz with $-10.68dB$ in accordance with the results obtained by the Matlab simulator.

3.4 Conclusions

Aim of this thesis work was to propose a new metasurface for ranging applications, able to focus the power in a certain region of space for improving the overall link efficiency for WEH scenarios. In the first chapter, after a brief introducion about the definition of metasurfaces, a deep investigation on the technologies presented in literarure have been conducted, in particular regarding the absorber and focusing metasurfaces. In the second chapter, a new design, starting from one of the solution investigated in the previous chapter, has been proposed. The design consist in 5x5 metasurface realized in PTFE with concentric geometry at 2.45 GHz. The unit cell exploited presents a celtic cross whose dimension changes based on the rings where it lays on: the correct tuning of these paramenters allows to properly define the

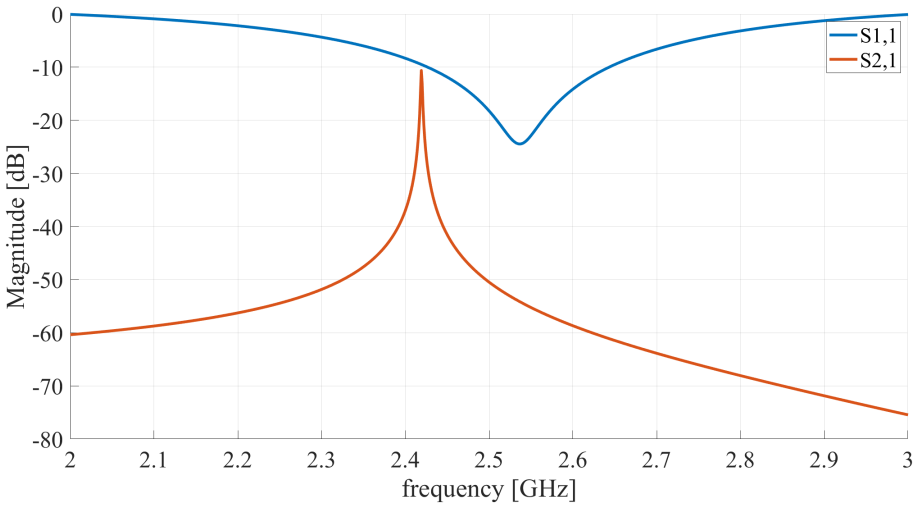

Figure 44: S parameters of the 2 antennas

focusing region. Since the overall size of the metasurface resulted very big, a compacted version of the metasurface involving 2 concentric rings has been proposed and its focusing properties has been compared with the previous solution. Finally, the wireless link performance has been analyzed. The plane wave excitation, untill here exploited for the design of the metasurfaces, has been replaced by the introduction oh a square patch antenna realized on PTFE operating at 2.45 GHz. Three different scenario for a 1 m link have been proposed:the absence of metasurfaces, therefore involving 2 identical patch antennas, the presence of the full metasurfaces composed by 3 rings and the one composed by 2 rings in front of the receiver patch, at the proper distance such that the receiver found in the maximum focusing region dictated by the metasurface. The simulated results have been calculated with the equivalence and reciprocity theorem. It has been highlighted the effect of the metasurfaces, in partcular the overall received power increases of 6.6 dB for the full surface, while the increment with the 2 rings model results 4.4 dB, respect to not exploit them. The goal has been reached, elevating the metasurfaces as an effective and easy-to-implement passive solution for increasing the overall efficiency for WPT or WEH applications. Future works will investigate on possibilities for size reduction of the overall metasurfaces such that it will be possible to obtain a compact and unique solution composed by the MS and the receiver patch.

References

[1] "Antennas for Wireless Systems" notes of the lectures of the course of A.A. 2021-22

[2] J. Zhou, P. Zhang, J. Han, L. Li and Y. Huang, "Metamaterials and Metasurfaces for Wireless Power Transfer and Energy Harvesting," in Proceedings of the IEEE, vol. 110, no. 1, pp. 31-55, Jan. 2022, doi: 10.1109/JPROC.2021.3127493.

[3] Chaimool, Sarawuth, and Yan Zhao. "Applications of Gradient Metasurfaces: A Review." ECTI E-Mag 11 (2017): 3-13.

[4] Fan Yu, Xuexia Yang, Huiteng Zhong, Chengyi Chu, Steven Gao; Polarization-insensitive wide-angle-reception metasurface with simplified structure for harvesting electromagnetic energy. Appl. Phys. Lett. 17 September 2018; 113 (12): 123903. https://doi.org/10.1063/1.5046927

[5] Liu, Yong-Qiang, et al. "Design and demonstration of a wide-angle and high-efficient planar metasurface lens." Optics Communications 474 (2020): 126061.

[6] Costanzo, A., Romani, A., Masotti, D., Arbizzani, N., & Rizzoli, V. (2012). RF/baseband co-design of switching receivers for multiband microwave energy harvesting. *Sensors and Actuators A: Physical*, *179*, 158-168.